The Meteoritical Society

Meteoritics & Planetary Science 44, Nr 11, 1755–1770 (2009)
Abstract available online at http://meteoritics.org

Vesta and the HED meteorites: Mid-infrared modeling of minerals and their abundances

Kerri DONALDSON HANNA[1, 2*] and Ann L. SPRAGUE[1]

[1]Lunar and Planetary Laboratory, University of Arizona, 1629 E. University Blvd., Tucson, Arizona 85721–0092, USA
[2]Present address: Department of Geological Sciences, Brown University, Box 1846, Providence, Rhode Island 02912, USA
[*]Corresponding author. E-mail: Kerri_Donaldson_Hanna@brown.edu

(Received 29 October 2007; revision accepted 12 August 2009)

Abstract–We demonstrate that the use of an established spectral deconvolution algorithm with mid-infrared spectral libraries of mineral separates of varying grain sizes is capable of identifying the known mineral compositions and abundances of a selection of howardite, eucrite, and diogenite (HED) meteorite samples. In addition, we apply the same technique to mid-infrared spectral emissivity measurements of Vesta that have been obtained from Cornell's Mid-Infrared Asteroid Spectroscopy (MIDAS) Survey and the Infrared Space Observatory (ISO). Each Vesta measurement was made over a different range of longitudes. Our spectral deconvolution results to the Vesta spectra corroborate that Vesta's surface is howardite or eucrite-like in composition and heterogeneous across its surface. The spectral fits produced by the linear deconvolution algorithm yields good results for the HED samples of known composition, thus giving us a high degree of confidence that our results for Vesta are valid.

INTRODUCTION

The goal of telescopic spectral measurements of remote planetary objects in the thermal infrared is to make mineral identifications to determine the object's composition and, perhaps, lead to a better understanding of its geologic history. Not only are high quality spectroscopic data required but also appropriate laboratory spectra for comparison and modeling are needed. Here we test our success at modeling mid-infrared spectra by using spectra from a select group of differentiated meteorites, the howardites, eucrites and diogenites (HEDs) of known composition and from the main belt asteroid Vesta, which has been suggested as a parent body to some HED meteorites. Previous studies linking the HED meteorites to Vesta have focused on visible- to near-infrared spectral measurements. Most asteroid observations have been made in the visible to near-infrared wavelength regime (0.4–2.5 μm) where absorption bands, band areas and spectral slope are used to determine pyroxene (clinopyroxene versus orthopyroxene) and olivine (forsterite versus fayalite) composition and surface maturity. In the near-infrared the common asteroidal surface materials that can be identified remotely include: pyroxene, olivine, phyllosilicates, organic material, and opaques (which include metallic iron, graphite, troilite, and magnetite) (Pieters and McFadden 1994).

Space weathering is a well-understood process for the lunar regolith, but is an active area of research for asteroids. The crucial question that must be answered regarding space weathering on asteroids is: is or has space weathering diminished spectral features so that they are no longer identifiable? The near-infrared spectra of Vesta and the Vestoids have relatively strong 1 μm features a fact inconsistent with reduced absorption bands owing to space weathering observed in lunar soils (Hiroi et al. 1994; Gaffey 2001). In the near-infrared, the optical effects of space weathering on the Moon are strongly linked to the development of nano-phase metallic iron in the soil (Pieters et al. 2001). It remains an open question, however, whether similar processes and products are possible on Vesta.

In this study we use the mid-infrared (8–14 μm) spectral region for identification of minerals and estimates of their abundances for a sample of three HED meteorites and Vesta. The use of the Christensen feature and silicate stretching bands (Reststrählen bands) in the mid-infrared are key in making plagioclase, pyroxene and olivine mineral identifications (major mineral phases for HED meteorites) as well as identifying minor phases including chromite, quartz, apatite, and troilite.

A well-established spectral deconvolution algorithm is used to determine minerals and abundances for each of the HED and Vesta spectra. Ramsey and Christiansen (1998)

demonstrated that a linear algorithm could be successfully used for making identifications using the diagnostic fundamental molecular vibration bands of minerals because at thermal wavelengths surface scattering dominates. Spectra for this study include a sample of HED meteorites measured by Salisbury et al. (1991) and remotely collected thermal emission spectra of Vesta. The HED meteorite samples were crushed and sieved to <70 μm grain size fractions. The mid-infrared spectra of Vesta were measured by the Mid-Infrared Asteroid Spectroscopy (MIDAS) Survey (Lim et al. 2005), low-resolution ground-based spectral measurements from 8.2–13 μm, and the Infrared Space Observatory (ISO) from 5.8 to 11.6 μm (Dotto et al. 2000). The laboratory spectra used in this study include spectral libraries from the Advanced Spaceborne Thermal Emission and Reflection Radiometer (ASTER) (Hook 1998), Brown University's Reflectance Experiment Laboratory (RELAB) (Pieters and Hiroi 2004), US Geological Survey (USGS) (Clark et al. 2007), Arizona State University spectral library (Christensen et al. 2000), and the Berlin Emissivity Database (BED) (Helbert et al. 2007; Maturilli et al. 2008).

Previous studies (Hamilton et al. 1997; Feely and Christensen 1999; Hamilton and Christensen 2000; Wyatt et al. 2001; Milam et al. 2007) have successfully used the same linear deconvolution algorithm on measured emissivity spectra of terrestrial and martian whole rock and coarse grain samples with spectral libraries of mineral separates of coarse grain size fractions (710–1000 μm). Hiroi et al. (1994, 1995) determined that Vesta's surface should be covered in fine grain fractions (<25 μm); therefore we built a spectral library of mineral separates of varying compositions and grain sizes, as they were available. We will show that the spectral deconvolution algorithm can be successfully used to model spectra of fine grain materials and surfaces using a spectral library built with appropriate mineral size separates. Using measurements from a previously unstudied spectral region we corroborate the link between the HED meteorites and Vesta making the link more robust. These results will either be supported or augmented when the Dawn mission arrives in 2011 (Russell et al. 2004, 2006).

Background

The HED Meteorites

The HED meteorites belong to the basaltic achondrite class, a related series of igneous rocks that are most like terrestrial basalts. The eucrites are formed during the crystallization of liquid on the parent body's surface and, therefore are crustal samples of the parent body. Eucrites typically are monomict or polymict breccias composed of basaltic clasts of variable coarseness set in a matrix of comminuted rock fragments (Keil 2002; Hutchinson 2004). They are primarily composed of low-calcium clinopyroxene (pigeonite with Mg# ~42–30), fine high-calcium exsolution lamellae, and high-calcium plagioclase (anorthite) with minor amounts of silica, chromite, ilmenite, Ni-poor kamacite, and troilite. The diogenites are believed to be formed as cumulates during fractional crystallization in magma chambers located deeper in the parent body's crust. Diogenites are monomict breccias with clasts of magnesium-rich orthopyroxene (hypersthene) in a matrix of comminuted grains of the same material. Diogenites contain ~84–100 vol% orthopyroxene (Mg# ~85–67) with minor amounts of olivine, chromite, calcium-rich pyroxene, calcium-rich plagioclase, troilite, Ni-poor kamacite and silica (Keil 2002; Hutchinson 2004). Howardites are polymict breccias comprised of magnesium-rich orthopyroxene, calcium-rich pyroxene, and calcium-rich plagioclase with minor amounts of Ni-poor kamacite, chromite, ilmenite, troilite, silica, and olivine. Howardites are most likely formed during an impact event into the parent body's surface. In fact, some howardites contain chondritic clasts that likely originate from the impacting body. Texturally the howardites are most like breccias found on the lunar surface.

Iron and Mn ratios of ferromagnesian silicates and oxygen isotopic ratios were used to genetically link the HED meteorites and confirm that they originated from a single differentiated body (Drake 2001). Iron and Mn behave very similarly in igneous events, but have very different volatilities. The differences in their volatilities lead to different initial abundances in planetary bodies. The Fe/Mn ratio can then be used as a planetary diagnostic if material originated from the same planetary body. Fe/Mn ratios for the HED meteorites fall along the same line therefore presumably originate from the same parent body. Oxygen isotopic ratios can be used in a similar fashion. Ratios for the HED meteorites clearly plot along their own line below the Earth-moon line. This indicates the three meteorite types have a common origin that is distinct from the Earth and the Moon (Drake 2001). Recently, improved laboratory instrumentation has allowed for higher precision oxygen isotopic analyses and two basaltic meteorites classified as eucrites (Ibitira and NWA cronos011) have been identified as having different oxygen isotopic signatures than that of the HED meteorites (Mittlefehldt 2005; Pieters et al. 2006). This suggests that there are at least two parent bodies one for the HED meteorites and another for the distinctive eucrites.

Vesta

Vesta is the third largest asteroid with a mean diameter of 516 km. It is the only large asteroid known to have a basaltic crust and has experienced significant heating and differentiation. Initially the asteroid 4 Vesta was linked to the HED meteorites (McCord et al. 1970; Larson and Fink 1975; Consolmagno and Drake 1977; McFadden et al. 1977; McFadden et al. 1981; Golubeva et al. 1983) after near-infrared spectroscopic measurements showed that Vesta's spectrum was unlike near-infrared spectra of other bright

asteroids such as Ceres and Pallas, but was similar to laboratory reflectance spectra of the HED meteorites. Like the HED meteorite spectra, Vesta's near-infrared spectrum has diagnostic pyroxene bands near 0.9–1.0 μm (Band I) and 1.9–2.0 μm (Band II) (Gaffey 1976; Gaffey 1997). The positions of Bands I and II are a function of the pyroxene composition (Adams 1974). Vesta's band minima are located between the band minima of the eucrites and diogenites, indicating an intermediate or "howardite-like" composition (Hiroi et al. 1994; Gaffey 1997; Pieters et al. 2006).

The Wide Field and Planetary Camera 2 (WFPC2) on the Hubble Space Telescope (HST) took images of Vesta using four filters to gain compositionally diagnostic information. Zellner et al. (1997) measured the albedo variations with rotation phase across Vesta's surface including the dark spot designated by Thomas et al. (1997) as the prime meridian. Binzel et al. (1997) observed color and albedo contrast between the eastern and western hemispheres suggesting a distinct difference in morphologies. Gaffey (1997) used high precision spectrophotometry of Vesta to map the surface heterogeneity and hypothesized that a circular region of approximately 150 km radius (~10% of Vesta's surface) is an olivine-rich location. A larger area would be required if the olivine is mixed in with other surface units. However, more detailed spectral measurements like those that will be made by the Dawn mission are needed for confirmation of these results. Thomas et al. (1997) used the Hubble Space Telescope to map Vesta's surface and found a large depression near the south pole that contained a central elevation and bounding rim. The northern hemisphere is smoother than the south and there is a real topographic difference between the hemispheres. Li et al. (2008) observed Vesta's southern hemisphere using the HST WFPC2 camera with the same four filters previously used to observe Vesta in 1994 and 1996. New measurements of the albedo agree with previous maps from 15 degrees South and 20 degrees North and new albedo features were observed.

Vesta's albedo (Degewij et al. 1979; Rivkin et al. 2005), near-infrared spectrum (Gaffey 1997; Vernazza et al. 2005), and the 506 nm spectral feature (Cochran and Vilas 1998; Vilas et al. 2000; Cochran et al. 2004) have been measured at various rotation phases. Vesta's surface properties vary from eastern to western hemisphere (Gaffey 1997; Binzel et al. 1997; Vernazza et al. 2005). Images show albedo variations and topography that are consistent with the known variations in Vesta's light curve (Rivkin et al. 2005) and the rotational differences in FeO band depths in the near-IR. The 506 nm absorption feature is a spin-forbidden Fe^{2+} in six-fold coordination (Vilas et al. 2000). This feature was measured at all rotation phases (Cochran and Vilas 1998; Vilas et al. 2000; Cochran et al. 2004) and the equivalent width of the feature varies across longitudes. Equivalent widths are significantly lower for the longitudes between 240 and 360 degrees and are high around 180 degrees. The region of low equivalent width is coincident with the large low albedo feature on the surface, which is a topographic high according to Thomas et al. (1997). Laboratory reflectance spectra of HED meteorites all show the 506.5 nm absorption band centered different wavelengths according to the pyroxene composition found in the meteorite sample (Hiroi et al. 2001). Hiroi et al. (2001) also showed that space weathering can remove or reduce the spectral contrast of the 506.5 nm absorption feature, but will not change its wavelength position.

Le Bertre and Zellner (1980) studied polarimetric, photometric, and spectroscopic properties of Vesta and a eucrite and concluded that Vesta's surface is best simulated by a broad mixture of particle sizes mainly <50 μm mixed and coated with particles of <10 μm. Hiroi et al. (1994, 1995) determined the particle sizes on Vesta's surface by comparing spectra taken over the 0.3–2.6 μm spectral range with laboratory spectra of HED meteorites powders of various grain sizes. The finest grain-size fraction (<25 μm) howardite powder has the closest match with Vesta in term of their overall reflectance spectra. Therefore, if the fine-grain howardite model of Hiroi et al. (1994, 1995) is correct, then additional space weathering is not required to produce the observed band strength of Vesta.

Association of HED Meteorites to Vesta

Although the association of the HEDs with Vesta was apparent, it was not clear what mechanism could transport material from the main-belt asteroid Vesta to Earth. The HST observations found a large impact crater in the southern hemisphere with a diameter of 460 kilometers (Thomas et al. 1997) that would have ejected approximately 10^6 km^3, which is more than the volume of the over 200 small asteroids that comprise the Vesta family (Burbine et al. 2001). Gaffey (1997) also found that all major classes of the HED meteorites are present as large geologic units on Vesta's surface. This discovery added another link between Vesta and the HEDs. Most of the observable surface is covered in polymict breccias, like howardites, but there are specific areas with spectral signatures of diogenites, low-calcium eucrites and olivine (Burbine et al. 2001). More recently McFadden et al. (2007) have imaged Vesta and obtained a detailed map of Vesta's surface that exhibits striking color differences thought to correspond to regions of different mineralogy.

Wisdom (1985) has shown that there is a large chaotic zone in the phase space near the 3:1 resonance and the chaotic trajectories within this zone could explain the dynamic mechanism needed to put objects into Earth crossing orbits. Cruikshank et al. (1991) found that three earth-approaching asteroids had spectra similar to Vesta and the HED meteorites. The spectral properties of the three small asteroids show them to be mineralogically very similar, if not identical, to at least some regions of Vesta, to the eucrites specifically, and the HEDs generally. The existence of several basaltic fragments on an Earth-approaching orbits helps ease the problem of the transport of fragments from an impact on Vesta to the vicinity

of Earth. Binzel and Xu (1993) answered the dynamical problem of getting material from Vesta to Earth. They discovered a number of smaller asteroids between Vesta and the meteorite supplying resonances such as the 3:1 and ν_6. These kilometer-sized bodies have visible spectra similar to Vesta (Burbine et al. 2001) and are named "the vestoids" because they are thought to originate from Vesta. Vilas et al. (2000) measured the 506 nm absorption feature in seven of the eleven vestoids measured by Binzel and Xu (1993) further linking the vestoids with Vesta. Binzel and Xu's (1993) work provided the definitive empirical evidence that an impact into Vesta could eject large fragments into resonances that are known for supplying meteorites into Earth-crossing orbits.

Mid-Infrared Spectral Interpretation

Plagioclase feldspars, major mineral constituents of asteroids and meteorites, often do not have diagnostic features in the near-IR and Singer (1981) demonstrated that large amounts (at least 50 weight percent) of olivine must be in an intimate mixture to be detectable in the near-IR. Low- and high-Ca pyroxenes have diagnostic spectral bands in the near-IR at 1 and 2 μm, but when there are mineral assemblages that contain both low- and high-Ca pyroxenes advanced band-fitting procedures are used to make unambiguous pyroxene identifications. In contrast, Lyon (1965) demonstrated that the fundamental molecular vibration bands (from 8–14 μm) of silicate minerals, in particular olivine, low- and high-Ca pyroxenes and feldspars, in fine particulate assemblages have detectable diagnostic spectral bands. These diagnostic bands, also known as Restsstrählen bands, can be diminished or exaggerated in spectral contrast due to thermal gradients, space weathering, shock effects, and particle size, but do not disappear (Salisbury et al. 1991). Sprague et al. (1994) demonstrated that as powders are heated or cooled their spectral slope changes and spectral features might change in band depth but do not disappear or change in wavelength location. More detailed measurements of many minerals and rock compositions including feldspar, over a range of grain sizes, has corroborated and expanded those results (Helbert et al. 2007; Maturilli et al. 2008)

Mustard and Hays (1997), and Clark (1999) demonstrated that in the mid-infrared where surface scattering dominates, as grain size decreases significant scattering is introduced because a small amount of energy is lost to absorption during each of the multiple reflections that take place among the grains. Therefore as the grain size decreases the spectral shape and contrast of the Reststrahlen bands also decrease, but the fundamental band centers remain constant. The Christensen feature (7.5–9 μm) and transparency maxima (11–13 μm), diagnostic features of silicates, become more prominent as grain size decreases (Cooper et al. 2002). Transparency features are observed to exhibit several systematic changes with these small particle size separates. In general, the feature shows an increase, and then a decrease in spectral contrast, the wavelength position of the reflectance maximum typically shifts to shorter wavelengths, and the features show a change in symmetry. Because of the non-linear effects of surface scattering for small grain size fractions (Mustard and Hays 1997) it is difficult to model spectra of mineral assemblages unless the spectral library being used contains mineral spectra of fine grain size fractions that are similar in size to those in the mineral assemblages (Ramsey and Christensen 1998). In this analysis, laboratory reflectance spectra of both fine- and coarse-grain minerals are used in the spectral deconvolution to take advantage of the increased spectral information in the fundamental absorption bands and to decrease RMS errors in modeling the best fits to each spectrum.

ANALYSIS

Spectra Used for This Study

Meteorite

Three meteorites were chosen from the Salisbury et al. (1991) spectral library (a howardite, eucrite and diogenite) for analysis here: Bholghati (USNM No. 1250), Haraiya (USNM No. 5702), and Johnstown (USNM No. 3419), respectively. The chosen meteorites have been well characterized in the laboratory (Floran et al. 1977, 1981; Fuhrman and Papike 1981; Kitts and Lodders 1998; Schwartz and McCallum 2001).

Bholghati is a polymict breccia composed of a diverse set of pyroxene compositions. The meteorite fell in Orissa, India in 1905. Fuhrman and Papike (1981) analyzed the bulk composition of Bholghati and determined that it contained 36–42% low-calcium pyroxene ($Wo_{0–15}En_{25–65}Fs_{35–75}$), 24–28% high-calcium pyroxene ($Wo_{15–40}En_{45–65}Fs_{35–55}$), 18–23% plagioclase ($An_{85–93}$), and trace amounts of ilmenite, chromite, olivine (Fo90–Fo80), silica, and Ni-Fe metal. Reid et al. (1990) found several carbonaceous clasts in the Bholghati sample that texturally resemble CM2 meteorites. The carbonaceous clasts had a composition of low-iron olivine (forsterite) and pyroxene (clinoenstatite) and minor amounts of low-iron augite.

Haraiya is a monomict, brecciated eucrite that fell in the Basti District, Urrat Pradesh, India, in 1878. Kitts and Lodders (1998) compiled previous laboratory measurements of Haraiya's composition and found that it was composed of 59.2% pyroxene ($Wo_{12}En_{34}Fs_{52}$), 35.4% plagioclase ($An_{89}Ab_{10}Or_1$), 1.0% ilmenite, 0.4% chromite, 0.2% apatite, and 2.4% quartz. Schwartz and McCallum (2001) found that Haraiya was composed of fine- to medium-grained basaltic clasts in a brecciated matrix with three distinct clast textures. Schwartz and McCallum used a JEOL 733 Superprobe to determine the major and minor element compositions of all phases in each of the three clast textures. The first clast texture, type A, was composed of fine-grained plagioclase laths partially enclosed in pyroxene grains to 200 μm. Modal analysis of the major and minor phases yielded a composition

of 40.1% plagioclase ($An_{86.3}$–$An_{92.3}$), 30% pyroxene (pigeonite as exsolution and host) ($Wo_{1.8}En_{35.7}Fs_{62.5}$), 19.4% pyroxene (augite as exsolution and host) ($Wo_{43.2}En_{28.7}Fs_{28.1}$), 10.5% silica with minor amounts (~1%) of troilite, ilmenite, chromite, and apatite. Clast texture type B was found to be coarser-grained clasts consisting of 50% pyroxene (pigeonite with exsolved augite lamellae) ($Wo_{1.7}En_{35.4}Fs_{62.9}$), 45% plagioclase ($An_{86.0}$–$An_{92.29}$), and <5% pyroxene (augite with pigeonite exsolution lamaellae) ($Wo_{43.9}En_{29.2}Fs_{26.8}$). Type B pyroxenes appear clouded in transmitted light likely due to opaque micro-inclusions of ilmenite, chromite, troilite and kamacite. Clast texture type C was composed of single pigeonite oikocrysts to 3 mm enclosing numerous block plagioclase grains that average 100 μm. Type C clasts had the highest modal abundance of pyroxene (pigeonite) ($Wo_{1.8}En_{36.6}Fs_{61.6}$) to plagioclase ($An_{95.3}$–$An_{97.2}$) ratio, 60:40.

The Johnstown meteorite fell in 1924 in north-central Colorado and is a brecciated ultramafic rock composed chiefly of angular to subrounded clasts of orthopyroxene in a variably comminuted matrix of the same material (Floran et al. 1977, 1981). Floran et al. studied seven polished thin sections as well as the largest hand specimen from the Johnstown meteorite and measured the mineral phases using an ARL-EMX SM electron microprobe. The brecciated and unbrecciated portions were found to be identical in bulk chemistry and mineralogy. Orthopyroxene ($Wo_{2.5}En_{73.5}Fs_{24}$) dominates with minor and accessory phases (in order of approximately decreasing abundance): plagioclase ($An_{86.7}Ab_{12.9}Or_{0.4}$), troilite, tridymite, olivine ($Fo_{71.3}$), metallic nickel-iron, clinopyroxene ($Wo_{46.4}En_{44.4}Fs_{9.3}$), and chromite. The plagioclase and olivine phases were found in only one of the thin sections studied.

Salisbury et al. (1991) measured a collection of meteorites laboratory using a Nicolet 5DXB FTIR spectrophotometer at 4 cm^{-1} constant spectral resolution throughout the spectral range (2.1–25 μm). Further description of the instrumental set-up can be found in Salisbury et al. (1987, 1991). The powder samples for our chosen meteorites were provided by Eugene Jarosewich of the United States National Museum (Smithsonian) (USNM). The USNM samples passed through a 75 μm sieve screen, however details of the particle size range of individual samples were not determined. It is difficult to know if this grain size range represents the grains found in the asteroid regolith. However, if the larger grains in the asteroid regolith are coated with fines, the fine grains dominate the spectral properties in the region of surface scattering (Salisbury et al. 1991). Therefore the meteorite samples are appropriate analogues for asteroids. These laboratory reflectance spectra are available in the ASTER spectral library. The biconical reflectance spectra for the chosen HED meteorites are shown in Fig.1.

Vesta

Spectral emissivity measurements of Vesta were made by Dotto et al. (2000) using the Infrared Space Observatory (ISO) and Lim et al. (2005) using the Cornell Mid-Infrared Asteroid Spectroscopy (MIDAS) Survey. The ISO uses the imaging photopolarimeter ISOPHOT, in particular the subsystem PHT-S which consists of two low-resolution grating spectrometers which cover the wavelength ranges 2.5–4.9 μm (PHT-SS) and 5.8–11.6 μm (PHT-SL). Measurements of Vesta and other Main Belt asteroids were made on 13 June 1997. Observational parameters for the ISO Vesta measurements are in Table 1. The ISO Vesta spectrum shows strong spectral features with approximately 10% overall spectral contrast with local uncertainties of 3–5%. In particular there is a 10% absorption feature centered at 10 μm.

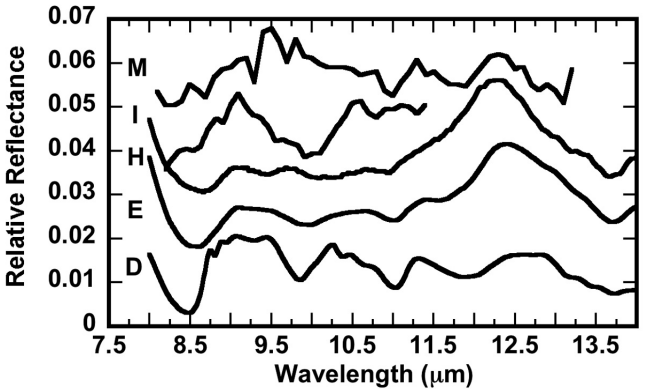

Fig. 1. Spectra of (M) MIDAS Vesta observed on 2 October 2001 at sub-solar latitude 7° and west longitude 73–96°, (I) ISO Vesta observed on 13 June 1997 at sub-solar latitude −19° and west longitude 221°, (H) Bholghati, (E) Haraiya, and (D) Johnstown. Meteorite spectra H, E, and D are from Salisbury et al. (1991) and grain size <70 μm. Spectra have been offset to distinguish similarities and differences between each.

MIDAS collected spectral measurements from 8.2–13 μm of 29 asteroids at Palomar Observatory using the 200-inch Hale telescope with the Spectrocam-10 in low-resolution mode. Spectral measurements of Vesta were made on two consecutive nights 2 and 3 October 2001. Observational parameters for the MIDAS Vesta measurements are in Table 1. The best spectral measurements achieved detection of subtle (2–3 % spectral contrast) features on Vesta consistent from night to night. MIDAS Vesta spectra have spectral features with no greater than 4% overall spectral contrast with local uncertainties of less than 2%. A more detailed discussion on the source of local uncertainties can be found in Lim et al. (2005). For this analysis, only the MIDAS Vesta spectrum from 2 October 2001 was used because the average local uncertainties are smaller than that of the 3 October 2001 spectrum. The strong spectral features, in particular the 10% minimum centered at 10 μm, observed in the ISO Vesta spectrum are absent from the MIDAS spectra of Vesta. However the MIDAS and ISO spectral measurements cover different fields of view on Vesta's surface. Lim et al. (2005) used the Thomas et al. pole solution to calculate the footprints of the MIDAS and ISO observations and place them on a Cartesian grid of Vesta's surface (Fig. 2).

Table 1. Observational parameters for Vesta measurements taken from Lim et al. (2005).

Observation	Date	Time (UTC)	Sub-solar point Lat.	Sub-solar point W. long	Sub-Earth point Lat.	Sub-Earth point W. long
ISO	13 June 1997	13:57:53	−19°	221°	−11°	198°
MIDAS	2 Oct 2001	10:40	7°	73°	18°	56°
MIDAS	2 Oct 2001	11:00	7°	96°	18°	78°
MIDAS	3 Oct 2001	11:00	7°	273°	18°	256°
MIDAS	3 Oct 2001	11:40	7°	317°	18°	300°

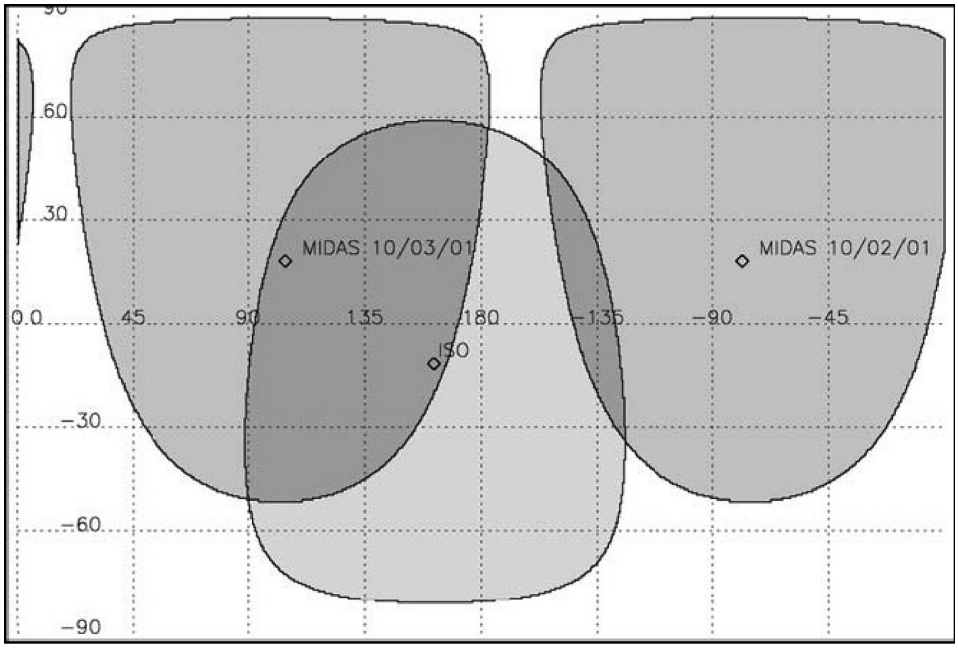

Fig. 2. A cylindrical projection of Vesta's surface on a grid of ±90 degrees of latitude and 0–360 degrees of longitude. The grey footprints represent seventy degree fields of view for the sub-Earth points for the MIDAS and ISO observation times. Figure is from Lim et al. (2005).

Spectral flux measurements of Vesta were calibrated into emittance by ratioing the measured asteroid spectrum to a fitted standard thermal model spectrum (Dotto et al. 2000; Lim et al. 2005). The emittance spectra were then converted to reflectance using Kirchoff's approximation (Reflectance = 1–Emittance) to make them comparable to the HED and mineral laboratory reflectance spectra. The MIDAS and ISO spectral measurements are plotted along with the Salisbury et al. (1991) HED spectra in Fig. 1. Several of the spectral features in the MIDAS Vesta spectrum are similar to features in the HED spectra, in particular the reflectance maximum near 12.25 μm and the reflectance minimum near 11 μm. The fundamental bands in the MIDAS Vesta spectrum are located at wavelengths between the locations of the fundamental bands in the Bholghati (howardite) and the Haraiya (eucrite) spectra.

Spectral Deconvolution

Description

Ramsey and Christensen (1998) developed a spectral deconvolution algorithm that is based on the principle that the emitted or reflected energy from a multi-mineralic surface is a decipherable combination of the energy radiated from each component in proportion to its areal percentage. For the assumption of linearity with respect to spectral mixing, the areal percentage of surface minerals with known particle sizes and densities translates into the volume present. Inputs into the spectral deconvolution algorithm include a spectrum to be unmixed, a spectral library of end-members (minerals) measured at the same wavelengths as the input spectrum, and the wavelengths over which to model. Outputs of the algorithm include a best fit model spectrum, the percentages of the end-member minerals used in the best fit model, and a root-mean square (RMS) error. The RMS error is an average error over the entire spectral range and is not necessarily a good indicator of how good the fit is. A residual model spectrum can be generated with each best fit model spectrum. The residual model spectrum is the best model fit subtracted from the mixed spectrum and provides a clearer picture of which regions of the spectrum is being fit well and which regions are not. A blackbody (Hamilton et al. 1997) (unity at all wavelengths) can also be added to the deconvolution to accommodate variations in the spectral contrast between the input spectrum and the best model fit. A blackbody reduces

the spectral contrast uniformly across the spectrum but does not change the spectral shapes or band positions. In every spectral deconvolution that we performed the blackbody was added to improve the best model fits.

The spectral fit is only as good as the spectral library used in the deconvolution. A spectral library built with as many mineral compositions at varying grain-size fractions can be built as they are measured in the laboratory but it is unlikely that those end-members in the spectral library will be the exact composition and grain size found in an unknown rock on a remotely sensed planetary body. If an exact mineral composition and/or grain size is absent from the spectral library end-members chosen for the best model fit will likely be inflated for the summation of end-members to equal unity. Hamilton and Christensen (2000) found that in many cases the best model fit included several end-members from within a solid solution series (i.e., plagioclase and pyroxene). Because it is probable that none of the spectral end-members represents exactly the same composition as a mineral in a given rock, it seems logical that multiple end-members may be used in the fit in order to reproduce the spectral composition of a real mineral with a composition of a mineral somewhere in between. Hamilton et al. (1997) demonstrated this with fayalite and forsterite. Minor and trace constituents usually are not modeled because their contributions to the bulk spectrum are unresolvable.

Ramsey and Christensen (1998) generated laboratory mixes with varying abundances of hornblende, microcline, oligoclase, and quartz and performed a blind retrieval test by selecting all end-members to be fit. Results for the blind retrieval test showed that for each mineral in the mixture differences between the unmix model abundance and the actual abundance could be as great as 12%, but the average difference was 4%. For some of the laboratory mixtures, the unmix model fit minerals that are not present in the laboratory mixture, but these are fit with abundances of less than 5%. This indicates that the linear spectral deconvolution method can be used to predict mineral abundances to within 5%. These results are based on particle diameters <63 μm. As the particle diameters decrease the RMS error of the model fits increase, however with spectral libraries that contain mineral spectra of the appropriate size fraction the errors are reduced significantly (Ramsey and Christensen 1998).

Previous successes using the same spectral deconvolution algorithm include: Hamilton et al. (1997) fitting whole Martian meteorite samples representing the SNC meteorites, Feely and Christensen (1999) modeling whole rock samples that had previously been studied using petrographic techniques, Hamilton and Christensen (2000) modeling spectra of 20 igneous rocks of natural and cut surfaces, Wyatt et al. (2001) determining the phase abundances of whole igneous rocks and comparing the results with phase abundances determined by electron microprobe mapping, and Milam et al. (2007) modeling complex mixtures of plagioclase sands and other mineral phases. These studies of whole rock and coarse grain samples used spectral libraries built with large grain size mineral separates. At thermal infrared wavelengths spectra of large grain size fractions are nearly identical to spectra of whole rocks making them easier to model using a linear deconvolution algorithm.

Spectral End-Members

For this study, a spectral library of 337 end-members was constructed of fine- and coarse- grain size minerals that are known to be major and minor phases in the HED meteorites. End-members were downloaded from the ASTER, RELAB, USGS, BED and ASU spectral libraries. The goal was to build a spectral library that contained as many compositions and grain-size fractions for the known HED meteorite phases when available to make the spectral deconvolution results for this study the best possible. Several minor phases were not available to add to our compiled spectral library including Ni-Fe metal, silica (tridymite), and kamacite.

End-member spectra from the ASTER spectral library include laboratory reflectance spectra from two sources: Johns Hopkins University (JHU) (Salisbury et al. 1987) and the Jet Propulsion Laboratory (JPL) (Grove et al. 1992). JHU end-member samples were sieved into two grain-size fractions (0–74 μm and 74–250 μm) and reflectance measurements were taken at a resolution of 4 cm^{-1} over the 2.2–25.0 μm spectral range using a Nicolet* 5 DxB interferometer spectrometer. JPL end-member samples were sieved into three grain-size fractions (<45 μm, 45–125 μm, and 125–500 μm) and reflectance measurements were taken at a resolution of 4 cm^{-1} over the 2.2–25.0 μm spectral range using a Nicolet interferometer spectrometer. End-member samples in the RELAB spectral library (Pieters and Hiroi 2004) are of varying grain-size and are measured at a resolution of 4 cm^{-1} over the 2.0–25.0 μm spectral range using a Thermo Nicolet Nexus 870 spectrometer. End-member samples of varying grain-size fractions from the USGS spectral library (Clark 2007) were measured using a Nicolet Fourier Transform Infra-Red (FTIR) interferometer spectrometer covering the spectral range from 1.3–150 μm at a resolution of 2 cm^{-1}. BED end-member samples are sieved into four grain-size fractions (<25 μm, <63 μm, 63–90 μm, and 90–125 μm) and thermal emission spectra are collected at a resolution of 4 cm^{-1} over the 6.3–22.0 μm spectral range using a Fourier transform infrared spectrometer (Maturilli et al. 2008). ASU end-member samples are of a single grain-size (710–1000 μm) and thermal emission spectra are collected at a resolution of 2 cm^{-1} over the 2.0–25.0 μm spectral range using a Mattson Cygnus 100 interferometric spectrometer (Christensen et al. 2000).

Thermal emission spectra taken from the BED and ASU spectral libraries were converted to reflectance using Kirchoff's law (Emissivity = 1–Reflectance), a well-known relationship that is regularly used in remote sensing

Table 2. Measured and model-derived modal mineral abundances for Bholghati, Haraiya, and Johnstown.

	Bholghati[a]		Haraiya[b,c]		Johnstown[d]	
Mineral type	Measured	Model	Measured	Model	Measured	Model
High-Ca pyx	24–28	24	<15	70	<3	
Low-Ca pyx	36–42	48	50–60		80–90	81
Plagioclase	18–23	19	35–45	30	<3	3
Olivine	<2	2			<3	17
Chromite	<2	7	<1		<3	
Ilmenite	<2		<1			
Troilite					<3	
Apatite			<1			
Quartz			<3			

Low-Ca pyx category includes orthopyroxene and/or pigeonite. Values are in units of vol%.
[a]Fuhrman and Papike (1981).
[b]Kitts and Lodders (1998).
[c]McCallum and Schwartz (2001).
[d]Floran et al. (1977, 1981).

Table 3. Model-derived modal mineral abundances for Vesta.

	Vesta	
Mineral type	ISO	MIDAS
High-Ca pyx	10	19
Low-Ca pyx	23	58
Plagioclase	45	7
Olivine	14	<1
Chromite	<5	14
Quartz	<2	
Apatite		<1

Low-Ca pyx category includes orthopyroxene and/or pigeonite. Values are in units of vol%.

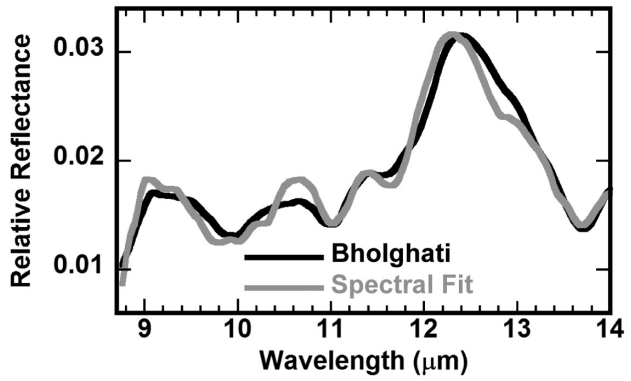

Fig. 3. The Bholghati reflectance spectrum plotted along with the deconvolved spectrum. The spectral fit contained 48% low-Ca pyroxene (pigeonite and hypersthene), 24% high-Ca pyroxene (augite), 19% plagioclase (anorthite), and minor amounts of chromite and olivine (Fo89). The Bholghati spectrum is from the ASTER spectral library with grain size <70 μm.

applications (Salisbury et al. 1994). All 337 end-member spectra were then interpolated for identical spectral sampling as the HED meteorites and Vesta spectra as described in 3.1. Recent work by Moroz et al. (2007) shows that for loose powders measured at ambient pressures emissivity spectra of minerals and biconical reflectance spectra of the same minerals do not deviate from one another by more than 3%. However, for coarse-grained mineral separates transparency features visible in the emissivity spectra are missing from the biconical reflectance spectra. Moroz et al. also showed that for slabs and compact fine powders there were non-systematic significant differences between the emissivity and biconical reflectance spectra. For this study where fine-grain mineral separates dominate the spectra of the HED meteorites and Vesta the Kirchoff approximation is of valid use. However we do note that the possible 3% deviation in band contrast of spectral features in the emissivity and reflectance spectra complicates the linear unmixing because differences in grain sizes also changes the band contrast in spectral features.

Observations of the large impact crater in the southern hemisphere by the Hubble Space Telescope suggest that shock metamorphism played an important role on Vesta's surface. The effect of shock metamorphism to the spectral contrast of the Reststrahlen bands is currently an active area of research. Pyroxenes and plagioclase feldspars are shocked in the laboratory and then spectral measurements are made (Johnson et al. 2002; Johnson and Hörz 2003). In the future, spectra of shocked materials will be included in the spectral libraries used for making mineral identifications in asteroid and meteorite spectra, but are not included for this analysis.

Results

The results of the spectral unmixing for Bholghati, Haraiya, Johnstown, and Vesta are shown in Tables 2 and 3 and Figs. 3, 4, 5, 6, and 7. Table 4 compares the compositions of the minerals in the meteorites to the compositions of the deconvolved minerals. Major and minor mineral chemistries for the minerals chosen in this study (meteorite and Vesta models) are shown in Table 5.

Bholghati

The best spectral fit is found using the primary minerals for a howardite meteorite (low- and high-Ca pyroxene and

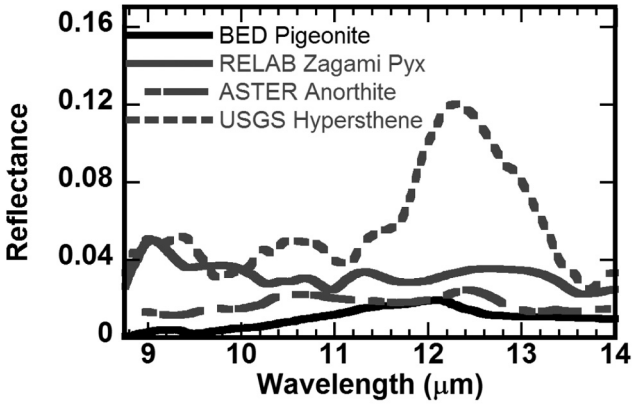

Fig. 4. The major phase end-members in the modeled Bholghati meteorite spectrum that contribute >10 vol%. End-members include BED pigeonite of grain size 25–45 μm, RELAB Zagami pyroxene of grain size 0–50 μm, ASTER anorthite.1f of grain size 0–74 μm, and USGS hypserthene (PYX02) of grain size <250 μm.

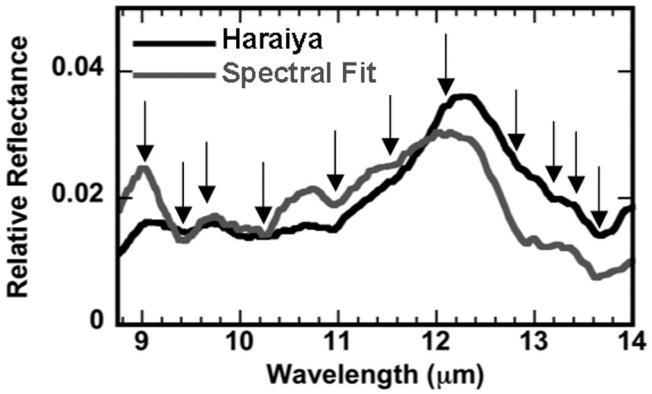

Fig. 5. The Haraiya reflectance spectrum plotted along with the deconvolved spectrum. The spectral fit contained 70% high-Ca pyroxene (Zagami pyroxene and augite) and 30% plagioclase (anorthite). The Haraiya spectrum is from the ASTER spectral library with grain size <70 μm. Arrows indicate a match in spectral band locations. Obvious artifacts owing to grain size are present.

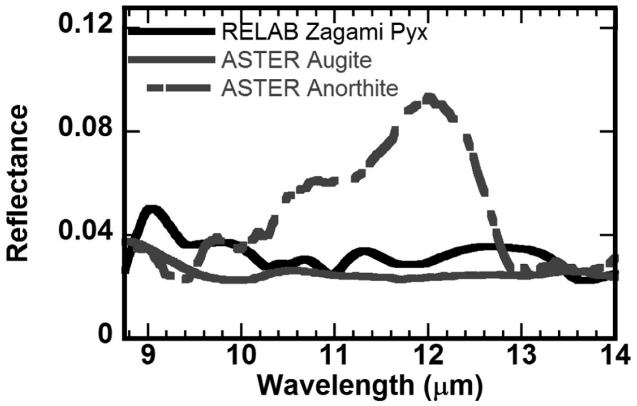

Fig. 6. The major phase end-members in the modeled Haraiya meteorite spectrum that contribute >10 vol%. End-members include RELAB Zagami pyroxene of grain size 0–50 μm, ASTER augite.2f of grain size 0–74 μm, and ASTER anorthite of grain size 0–45 μm.

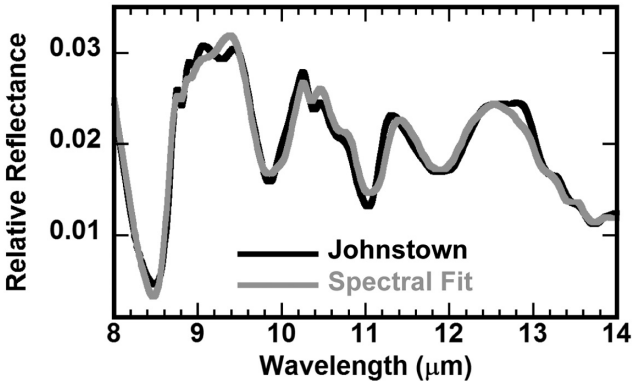

Fig. 7. The measured Johnstown reflectance spectrum plotted along with the deconvolved spectrum. The spectral fit contained 81% of low-Ca pyroxene (hypersthene), 17% olivine (Fo_{88} and Fo_{18}) and 3% plagioclase (anorthite). The Johnstown spectrum is from the ASTER spectral library with grain size <70 μm.

plagioclase feldspar) with minor amounts of chromite and olivine (Fo_{89}) (Fig. 3). The major phase end-members (greater than 10 vol%) are plotted in Fig. 4. The best model fit mineral percentages match to within approximately 0–5% of the published data for Bholghati (Table 2). Howardites are polymict breccias that are mixtures of both surface eucritic material and internal diogenitic material. Polymict breccias are composed of diverse mineral and lithic clasts (Mittlefehldt et al. 1998); therefore mineral phases and abundances determined by optical or electron microprobe mapping techniques are highly dependent on the sample measured. This should be kept in mind when comparing the resulting modes and abundances from the spectral deconvolution algorithm with those measured in the laboratory. The deconvolved mineral modes and abundances for the Bholghati spectrum fit within the definition of a howardite meteorite.

Major minerals chosen in the best model fit included low-Ca pyroxene, high-Ca pyroxene and plagioclase. Two low-Ca pyroxenes were chosen: a BED pigeonite with a grain size fraction of 25–45 μm and USGS hypersthene (PYX02) with a grain size fraction of <250 μm. Compositions of both the pigeonite and hypersthene end-member samples fit within the large phase range measured by Fuhrman and Papike (1981). The deconvolution algorithm overestimated the modal abundance of low-Ca pyroxene by 6% over the measured range (Table 2). The high-Ca pyroxene chosen for the best fit model is a RELAB Zagami pyroxene with a grain size fraction of 0–50 μm. The modal abundance of high-Ca pyroxene (24%) determined by the deconvolution algorithm falls within the measured range. However the composition of the high-Ca pyroxene is more Ca-rich and less Mg-rich than the measured high-Ca pyroxene (Table 4). The fact that the high-Ca pyroxene chosen is not an exact match compositionally with the high-Ca pyroxene determined in the laboratory means that our spectral library is missing the necessary composition to best model the Bholghati spectrum.

Table 4. Compositions of major minerals in meteorite samples and model end-members.

	Bholghati[a]		Haraiya[b,c]		Johnstown[d]	
Mineral type	Measured	Model	Measured	Model	Measured	Model
High-Ca pyx	$Wo_{15–40}$ $En_{45–65}$ $Fs_{35–55}$	$Wo_{49}En_2Fs_{49}$	$Wo_{43–44}En_{28–29}$ $Fs_{27–28}$	$Wo_{42–49}En_{2–36}$ $Fs_{21–49}$	$Wo_{46–47}En_{44–45}$ $Fs_{9–10}$	
Low-Ca pyx	$Wo_{0–15}En_{25–65}$ $Fs_{35–75}$	$Wo_{0–25}En_{18–78}$ $Fs_{22–43}$	$Wo_{2–12}En_{34–37}$ $Fs_{52–63}$		$Wo_{2–3}En_{73–74}$ $Fs_{24–25}$	$Wo_{2–7}En_{58–78}$ $Fs_{22–39}$
Plagioclase	$An_{85–97}$	An_{99}	$An_{86–97}$	$An_{90–100}$	$An_{86–87}$	An_{99}
Olivine	$Fo_{65–90}$	Fo_{89}			$Fo_{71–72}$	Fo_{88} and Fo_{18}

Low-Ca pyx category includes orthopyroxene and/or pigeonite.
[a]Fuhrman and Papike (1981).
[b]Kitts and Lodders (1998).
[c]McCallum and Schwartz (2001).
[d]Floran et al. (1977, 1981).

Table 5. Major and minor element analyses of end-members chosen in best fit models for Bholghati, Haraiya, Johnstown, and Vesta.

End-member	Source	Grain size (μm)	SiO_2	Al_2O_3	FeO	MgO	CaO	K_2O	Na_2O	TiO_2	MnO	Cr_2O_3
Apatite	ASTER	0–45										
Anorthite	ASTER	0–45										
Anorthite.1c	ASTER	75–250	43.53	0.02	0.02	0.03	19.26	0.04	0.03	0.01	0.03	
Anorthite.1f	ASTER	0–74	43.53	0.02	0.02	0.03	19.26	0.04	0.03	0.01	0.03	
Augite.1c	ASTER	75–250	48.93	8.44	8.59	14.37	16.87	0.02	1.57	1.38	0.21	
Augite.1f	ASTER	0–74	48.93	8.44	8.59	14.37	16.87	0.02	1.57	1.38	0.21	
Bytownite	BED	0–25										
Chromite.1c	ASTER	75–250	0.88	9.33	15.10	15.40	<0.02	<0.02	<0.15	0.10	0.24	60.66
Chromite 13	RELAB	0–45	0.02	6.99	11.94	12.16	0.03	0.00	0.00	0.05	0.31	63.10
Chromite 15	RELAB	0–45	0.02	17.07	13.23	13.44	0.01	0.00	0.00	0.36	0.29	51.28
Diopside.2f	ASTER	0–74	54.77	0.49	0.87	18.26	25.60	0.01	0.39	0.05	0.06	
Hypersthene.1c	ASTER	75–250	51.32	4.89	17.07	26.09	1.27	0.02	0.05	0.29	0.35	
Hypersthene.1f	ASTER	0–74	51.32	4.89	17.07	26.09	1.27	0.02	0.05	0.29	0.35	
Hypersthene	BED	25–63										
Hypersthene2	BED	0–25	51.68	6.46	10.56	24.59	2.57	0.16	1.02	0.593	1348*	
Hypersthene NMNHC 2368	USGS	0–74	51.32	4.89	17.07	26.09	1.27	0.02	0.05	0.29	0.35	
Hypersthene PYX02	USGS	10–20	55.30	0.12	9.38	32.80			0.00	0.05	0.15	
Magnesiochromite	ASTER	0–45										
Olivine.2f	ASTER	<60	31.11	0.00	59.75	7.71	0.09			0.06	1.30	0.07
Olivine.6f	ASTER	<60	35.47	0.00	34.63	29.49	0.09			0.03	0.55	0.04
Olivine.8f	ASTER	0–74	40.10	0.007	11.80	47.80	0.009			0.002	0.216	0.027
Olivine GDS70	USGS	<60	41.09		9.16	49.29	0.03			0.01	0.21	0.05
Olivine KI3005	USGS	<60	30.11	0.00	62.82	4.42	0.14			0.07	1.55	0.06
Olivine KI3054	USGS	<60	36.30		30.59	32.62	0.04			0.03	0.05	0.03
Olivine KI3188	USGS	<60	34.34		41.43	23.80	0.05			0.04	0.73	0.04
Pigeonite**	ASU	710–1000										
Pigeonite	BED	25–45	52.70	15.87	10.81	4.47	9.61	0.91	2.71	1.692	1228*	
Pigeonite	BED	45–63	52.70	15.87	10.81	4.47	9.61	0.91	2.71	1.692	1228*	
Zagami pyroxene	RELAB	0–50	51.10	0.00	16.05	0.87	16.10	0.00	14.35	0.41	0.58	0.54

*Values in units of ppm.
**Synthetic laboratory sample.

The overestimation of the modal abundance of low-Ca pyroxene could be a result of this compositional mismatch. The modeled plagioclase end-member is an ASTER anorthite with a grain size fraction of 0–74 μm. The composition of the anorthite end-member (An_{99}) is more calcium-rich than the measured plagioclase ($An_{85–97}$) (Table 4) and the modal abundance of plagioclase is within the measured range.

Minor minerals chosen in the spectral fit include olivine and chromite. Of the olivine end-members provided, the USGS olivine (GDS70) with a grain size fraction of <25 μm was selected. This olivine composition (Fo_{89}) is within the range of olivine clast compositions measured ($Fo_{65–90}$) however its abundance was overestimated by 1%. The 1% difference between the measured and modeled olivine is within the uncertainty associated with the linear deconvolution algorithm. The algorithm also chose ASTER

chromite with a grain size fraction of 75–250 μm. The deconvolved modal abundance is 6% greater than the measured modal abundance determined in the lab. This overestimation is likely a result of slight compositional differences in the high-Ca pyroxene and plagioclase. Although ilmenite end-members are provided in the spectral library none were chosen. Either the low modal abundance of ilmenite in the sample made it unresolvable in the spectrum or no ilmenite was present in the end-member sample from which the laboratory spectrum was collected. Reid et al. (1990) found several carbonaceous clasts in the Bholghati sample that texturally resemble CM2 meteorites. The carbonaceous clasts had a composition of low-iron olivine (Forsterite) and pyroxene (clinoenstatite) and minor amounts of low-iron augite. The spectral deconvolution algorithm did not fit any minerals that could be unambiguously identified with these carbonaceous clasts.

The spectral fit to Bholghati is encouraging (Fig. 3). The major minerals in the assemblage have been correctly identified as we can see that the maxima and minima in Bholghati's spectrum are at the same wavelength as in the spectral fit. Differences in grain size between those in the meteorite assemblage and those in the minerals in our spectral libraries are seen as amplitude differences in the spectral features at 9 and 11.8 μm. Differences in mineral composition between those in the meteorite assemblage and those in the minerals in our spectral libraries are seen as differences in band minimum from 9.8–10.1, 10.2–10.4 μm, and a mismatch of the reflectance peak at 12.2–12.4 μm.

Haraiya

The best spectral fit is found using the primary minerals for a eucrite meteorite including high-Ca pyroxene and plagioclase feldspar (Fig. 5). The major phase end-members (greater than 10 vol%) are plotted in Fig. 6. The linear deconvolution algorithm underestimated the plagioclase abundance (30% compared to the 35–45% measured in the laboratory), overestimated the abundance of high-Ca pyroxene by five times the measured value, and underestimated the low-Ca pyroxene by not choosing one (Table 2). Haraiya is a monomict breccia that is composed of three distinct basaltic clasts set in a matrix of variable coarseness (Schwartz and McCallum 2001). The major phases in a eucrite are low-Ca pyroxene (pigeonite) and high-Ca plagioclase with minor phases of silica, chromite, ilmenite, kamacite and triolite. Low-Ca pigeonite samples are difficult to find in nature and thus our spectral library lacks a good suite of compositions and grain size fractions for pigeonite. Thus the spectral fit to Haraiya's spectrum is limited by the lack of pigeonite compositions.

Major minerals chosen in the spectral fit include two high-Ca pyroxenes and plagioclase (Fig. 5). The high-Ca pyroxenes fit included the RELAB Zagami pyroxene of grain size fraction of 0–50 μm and ASTER augite.2f of grain size fraction 0–74 μm. The dominant low-Ca pyroxene phase measured was pigeonite (Schwartz and McCallum 2001), however the deconvolution algorithm did not chose any of the available pigeonite end-members. Our spectral library is missing the key pigeonite composition with the key grain size fraction. The missing phase is the dominant problem in fitting the eucrite spectrum. Also the chosen pyroxene, the RELAB Zagami pyroxene, is a pyroxene from a Martian meteorite, which has a distinctly different chemistry than eucritic pyroxenes. This clearly indicates that our spectral library is missing a high-Ca pyroxene that is similar in chemical composition to the Haraiya high-Ca pyroxene. It also demonstrates a weakness in the spectral deconvolution method in that it will choose a mineral even if it is clearly a bad choice composition-wise. As our spectral library grows with varying mineral compositions and grain size fractions this will become less of an issue. Schwartz and McCallum (2001) did measure augite in their Type A and B clasts, but the highest modal abundance of 19% was only found in the Type A clasts. The highest modal abundance of augite is still 11% less than the modal abundance of augite as determined by the best model fit. Of the plagioclase end-members provided, the ASTER anorthite end-member of grain size fraction 0–45 μm was chosen. The composition of the anorthite end-member within the range of the measured plagioclase (Table 4) and the modal abundance of plagioclase is overestimated by 5%.

Although our spectral library does contain spectra of the measured minor phases quartz, ilmenite and chromite, the spectral deconvolution algorithm did not fit them to the Haraiya spectrum. Either the low modal abundance of minor phases in the Haraiya sample made it unresolvable in the spectrum or spectra from the minor phases present in the end-member spectral library did not reproduce those of the meteorite.

There are obvious differences between the Haraiya spectrum and the spectral deconvolution fit due to mineral composition and grain size differences (marked by arrows in Fig. 5). Salisbury et al. (1991) demonstrated that as grain sizes of minerals change spectral features can be exaggerated or diminished, however the wavelength location of the features does not change. Differences owing to grain size are seen from 8.75–9.2, 10.4–11.0, and 12.0–14.0 μm. Differences in mineral composition between those in the meteorite assemblage and those in the minerals in our spectral libraries are seen as differences in band minimum 11.0 μm, and a mismatch of the reflectance peak at 12.2–12.4 μm.

Johnstown

The best spectral fit is found using the primary mineral for a diogenite (low-Ca pyroxene) with minor amounts of plagioclase and olivine (Fo_{88} and Fo_{18}) (Fig. 7). The deconvolved modal abundances for low-Ca pyroxene and plagioclase are within the published data range for Johnstown, however the olivine abundance is overestimated

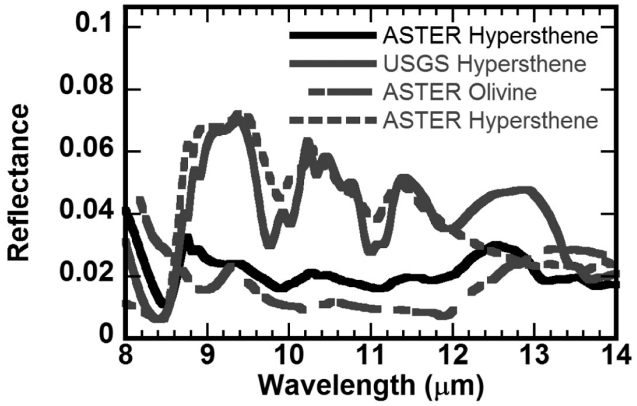

Fig. 8. The major phase end-members in the modeled Johnstown meteorite spectrum that contribute >10 vol%. End-members include ASTER hypersthene.1f of grain size 0–74 μm, USGS hypersthene (PYX02) of grain size 104–150 μm, ASTER olivine.8f of grain size 0–60 μm, and ASTER hypersthene.1c of grain size 75–250 μm.

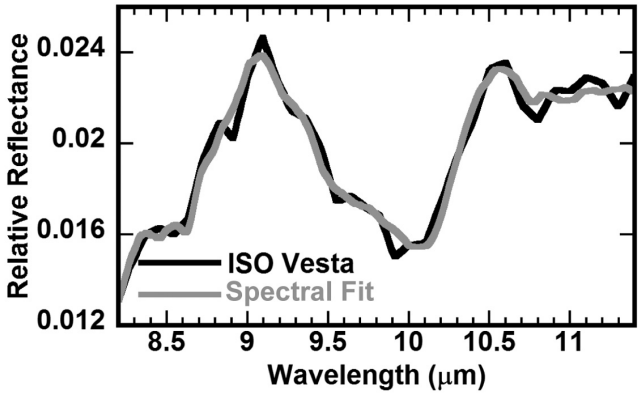

Fig. 9. The measured ISO Vesta reflectance spectrum plotted along with the deconvolved spectrum. The ISO spectral measurement was made at sub-solar latitude of –19° and west longitude of 221° (Lim et al. 2006). The spectral fit contained 10% high-Ca pyroxene (augite), 23% low-Ca pyroxene (pigeonite and hypersthene), 45% plagioclase (anorthite and bytownite), 14% olivine (Fo_{60}, Fo_{11} and Fo_{89}) and minor amounts of chromite and quartz.

by more than five times that measured in the laboratory (Table 2). Johnstown is the largest representative by mass of the diogenite class of meteorites (Floran et al. 1981). Diogenites are dominated (approximately 84–100 vol%) by orthopyroxene with minor minerals (approximately 0–5 vol%) chromite and olivine and accessory minerals (approximately 0–2 vol%) diopside, triolite, metal, a silica phase, and rare phosphates (Mittlefehldt et al. 1998). The spectrally derived mineral modes and abundances for Johnstown fit within the definition of a diogenite meteorite.

Major and minor phases chosen in the spectral fit include a suite of low-Ca pyroxenes, plagioclase and two modes of olivine. The major phase end-members (greater than 10 vol%) are plotted in Fig. 8. The low-Ca pyroxenes fit include ASTER hypersthene.1f of grain size fraction 0–74 μm,

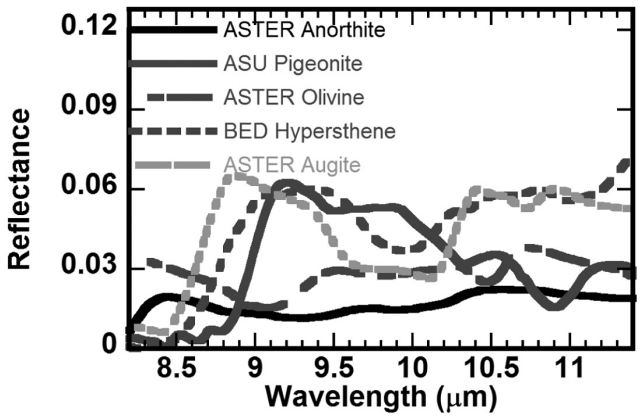

Fig. 10. The major phase end-members in the modeled ISO Vesta spectrum that contribute >10 vol%. End-members include ASTER anorthite.1f of grain size 0–74 μm, ASU pigeonite of grain size 710–1000 μm, ASTER olivine.6f of grain size 0–60 μm, BED hypersthene (2) of grain size 0–25 μm, and ASTER augite.1c of grain size 75–250 μm.

USGS hypersthene (PYX02) of grain size fraction 120 μm, ASTER hypersthene.1c of grain size fraction 75–250 μm, BED hypersthene of grain size fraction 25–63 μm, USGS hypersthene (PYX02_ of grain size fraction <250 μm, and USGS hypersthene (NMNHC) of grain size fraction 0–74 μm. The three with the highest abundances are ASTER hypersthene.1f (42%), USGS hypersthene (PYX02) (17%) and ASTER hypersthene.1c (13%). Compositions of all the hypersthene end-member samples fit within the phase range measured by Floran et al. (1977, 1981) (Table 4). The fact that multiple hypersthene end-members were chosen indicates that our spectral library does not contain the correct composition and/or grain size fraction for hypersthene. Hamilton et al. (1997) used fayalite and forsterite end-members to show that the spectral deconvolution algorithm will chose multiple end-members of varying composition when the exact mineral composition is missing. The modal abundance of all hypersthene end-members combined is within the measured modal abundance range.

Minor minerals chosen in spectral fit include olivine and plagioclase. Of the olivine end-members provided, the ASTER olivine.8f and olivine.2f of grain size fraction <60 μm were chosen. One of the chosen olivine compositions (Fo_{88}) is more Mg-rich and the other (Fo_{18}) is more Fe-rich than the olivine clast compositions measured ($Fo_{71–72}$) and their combined abundance is more than five times greater than the abundance of olivine measured in the lab. The overestimation of the modal abundance of olivine could be a result of the olivine and low-Ca pyroxene compositional mismatches. The chosen plagioclase end-member is ASTER anorthite.1c with a grain size fraction of 75–250 μm. The composition of the anorthite end-member (An_{99}) is more calcium-rich than the measured plagioclase ($An_{86–87}$) (Table 4) and the modal abundance of plagioclase is within the measured range.

Our deconvolved spectrum is an excellent fit to the Johnstown meteorite (Fig. 7). The location, width and spectral contrast of the spectral features in the spectral fit are nearly the same as those in the Johnstown meteorite. However, the spectral contrast for some features in the spectral fit is not great enough to match features in the Johnstown spectrum.

Vesta

Vesta's spectrum was measured by ISO on 13 June 1997 (Dotto et al. 2000), covering the approximate longitudes 90° to −130° (Fig. 2). The deconvolution algorithm produces the best spectral fit (Fig. 9) with major phases (plagioclase, low-Ca and high-Ca pyroxenes) and minor phases (chromite, olivine and quartz). The major phase end-members (greater than 10 vol%) are plotted in Fig. 10. The plagioclase end-member chosen is the ASTER anorthite.1f of grain size fraction 0–74 μm. The low-Ca pyroxenes chosen include ASU pigeonite of grain size fraction 710–1000 μm and BED hypersthene (2) of grain size fraction 0–25 μm. The high-Ca pyroxene chosen is ASTER augite.1c of grain size fraction 75–250 μm. Olivine end-members chosen include ASTER olivine.6f (Fo_{60}) of grain size fraction <60 μm, USGS olivine (KI3005) (Fo_{11}) of grain size fraction <30μm, and USGS olivine (GDS70) (Fo_{89}) of grain size fraction 70 μm. The minor phase end-members chosen in the spectral fit include RELAB chromite of grain size fraction 0–50 μm and ASTER quartz.2c of grain size fraction 75–250 μm. The spectral deconvolution algorithm chose multiple olivine end-members because our spectral library does not contain the correct composition and/or grain size fraction of olivine. The deconvolved mineral phases and abundances (Table 3) covering the approximate longitudes 90° to −130° on Vesta's surface are indicative of a eucrite-like composition. The ISO Vesta spectrum has 3–5% local uncertainties and any end-member that has a modal abundance on the order of the local uncertainties should be considered carefully. Chromite and quartz are the minor phases that have modal abundances on the order of the local uncertainties. If these minor phases are not correctly chosen in the spectral fit the other phases chosen would still suggest a eucrite-like composition for this region on Vesta's surface.

MIDAS measured Vesta's spectrum on 2 October 2001 (Lim et al. 2005), covering the approximate longitudes −155° to 0° (Fig. 2). For this analysis, only the MIDAS Vesta spectrum from 2 October 2001 was used because the average local uncertainties are smaller than that of the 3 October 2001 spectrum. The deconvolution algorithm produces the best spectral fit (Fig. 11) with major phases (low-Ca and high-Ca pyroxenes) and minor phases (chromite, plagioclase, olivine and apatite). The major phase end-members (greater than 10 vol%) are plotted in Fig. 12. The low-Ca pyroxenes chosen include ASTER hypersthene.1f of grain size fraction 0–74 μm, BED pigeonite of grain size fraction 45–63 μm, and ASU pigeonite of grain size fraction 710–1000 μm. The high-Ca pyroxene chosen is RELAB Zagami pyroxene of grain size fraction 0–50 μm. Plagioclase end-members chosen include BED bytownite of grain size fraction 0–25 μm, ASTER anorthite of grain size fraction 0–45 μm, and BED bytownite of grain size fraction 63–90 μm. The minor phase end-members chosen in the spectral fit include ASTER magnesiochromite of grain size fraction 0–45 μm, ASTER chromite.1c of grain size fraction 75–250 μm, USGS olivine (KI3188) (Fo_{51}) of grain size fraction <25 μm, and ASTER apatite of grain size fraction 0–45 μm. The deconvolved mineral phases and abundances (Table 3) covering the approximate longitudes −155° to 0° on Vesta's surface are indicative of a howardite-like composition. The MIDAS Vesta spectrum has <2% local uncertainties and any end-member that has a modal abundance on the order of the local uncertainties should be considered carefully. Olivine and

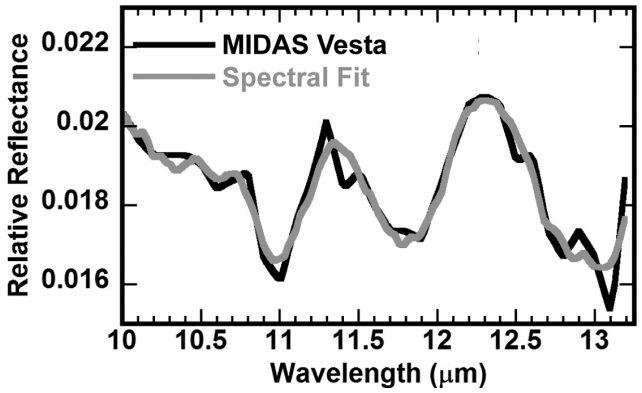

Fig. 11. The measured MIDAS Vesta reflectance spectrum plotted along with the deconvolved spectrum. The MIDAS spectral measurement was made at sub-solar latitude of 7° and west longitude of 73–96° (Lim et al. 2006). The spectral fit contained 19% high-Ca pyroxene (Zagami pyroxene), 58% low-Ca pyroxene (pigeonite and hypersthene), 7% plagioclase (anorthite), and minor amounts of olivine (Fo_{51}), chromite and apatite.

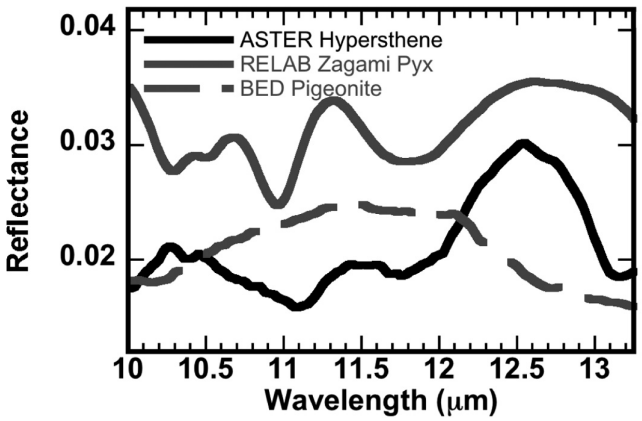

Fig. 12. The major phase end-members in the modeled MIDAS Vesta spectrum that contribute >10 vol%. End-members include ASTER hypersthene.1f of grain size 0–74 μm, RELAB Zagami pyroxene of grain size 0–50 μm, and BED pigeonite of grain size 45–63 μm.

apatite are the minor phases that have modal abundances on the order of the local uncertainties. Again, if these minor phases are not correctly chosen in the spectral fit the other phases chosen would still suggest a howardite-like composition for this region on Vesta's surface.

CONCLUSIONS

1. The spectral deconvolution algorithm fit the correct pyroxene and plagioclase compositions for the howardite and diogenite meteorite spectra. Also the plagioclase-to-pyroxene ratios for the HED spectral deconvolution fits compared well with the plagioclase-to-pyroxene ratios found from the laboratory analysis of the diogenite (Johnstown) and howardite (Bholghati) meteorite samples.
2. Our experience with modeling the HED meteorite spectra has given us confidence that the strengths of the spectral deconvolution algorithm outweigh its weakness. Strengths of the spectral deconvolution algorithm include: (1) when the approximate pyroxene composition is available in the library, pyroxene can be modeled within the measured abundance range and (2) plagioclase can be modeled within the measured abundance range. Weaknesses to this approach include: (1) if the correct composition or grain size of a mineral is missing the algorithm will either overestimate the abundances of other minerals or choose small abundances of random minerals to enable the total abundance of minerals to add up to 100, (2) if the correct composition or grain size of a mineral is missing the algorithm can choose a mineral with a different composition in an attempt to force a best fit model with the given minerals in the library, and (3) minor minerals (minerals with an abundance of less than 10%) are sometimes not chosen.
3. Spectral deconvolution of the MIDAS and ISO spectra corroborate that Vesta's surface composition is howardite or eucrite-like minerals and is heterogeneous. The best model fit to the MIDAS spectrum suggests that the surface location at approximate longitudes −155° to 0° is composed of fine-grain howardite-like minerals. The best model fit to the ISO spectrum suggests that the surface location at approximate longitudes 90° to −130° is composed of fine-grain eucrite-like minerals. Our pyroxene results confirm the near-infrared results. The deconvolution algorithm provides good estimates for the abundance of plagioclase and olivine. The abundance of plagioclase can be quite useful in distinguishing between eucrite and diogenite-like surfaces.
4. The best model fits to the howardite, diogenite, and Vesta spectra included olivine as minor phases (less than 10 vol%). This result corroborates Gaffey's (1997) high precision spectrophotometry results.
5. Once Dawn begins collecting spectral measurements at Vesta, our results using the spectral deconvolution will either be clarified or augmented.
6. The low-pressure surface environment of Vesta should create steep thermal gradients in the uppermost micrometers of the soil similar to the lunar environment. Thus the spectral deconvolution results will improve as minerals of varying grain size and compositions are measured under vacuum conditions and added to our spectral library. Our fits to the spectral emissivity measurements of Vesta should also improve as a library of thermal emission spectra of minerals of varying grain size is built.
7. New mid-infrared spectral measurements of Vesta taken from Earth-based or space-borne telescopes with a higher signal-to-noise and covering all of Vesta's rotation phases would greatly improve upon the current work. Also future improvements for the analysis of mid-infrared telescopic spectroscopic measurements using the spectral deconvolution algorithm should include spectral libraries with laboratory emissivity spectra of all pyroxenes and feldspars, shocked pyroxenes and feldspars, troilite and a range of Ni-Fe metals especially those measured under vacuum conditions.

Acknowledgments—We are very grateful to Michael Ramsey and Jen Piatek for provision of the spectral unmixing algorithm and help getting it running on our computers. The thorough reviews by Vicky Hamilton, Lucy McFadden, and Carlé Pieters are also greatly appreciated as it led to clarification of key issues in the manuscript. This research uses spectra acquired with: spectra reproduced from the ASTER Spectral Library through the courtesy of the Jet Propulsion Laboratory, California Institute of Technology, Pasadena, California. Copyright © 1999, California Institute of Technology, the NASA RELAB facility at Brown University, the USGS spectral library provided by Roger Clark (Clark et al. 2007), the Arizona State University spectral library (Christensen et al. 2000), and the Berlin Emissivity Database (Helbert et al. 2007). Donaldson Hanna and Sprague are grateful to the National Science Foundation through grant # AST 0406796 for this research.

Editorial Handling—Dr. Carlé Pieters

REFERENCES

Adams J. B. 1974. Visible and near-infrared diffuse reflectance spectra of pyroxenes as applied to remote sensing of solid objects in the solar system. *Journal of Geophysical Research* 79:4829–3836.

Binzel R. P. and Xu S. 1993. Chips off of asteroid 4 Vesta: Evidence for the parent body of basaltic achondrite meteorites. *Science* 260:186–191.

Binzel R. P., Gaffey M. J., Thomas P. C., Zellner B. H., Storrs A. D., and Wells E. N. 1997. Geologic mapping of Vesta from 1994 Hubble Space Telescope images. *Icarus* 128:95–103.

Burbine T. H., Buchanan P. C., Binzel R. P., Bus S. J., Hiroi T., Hinrichs J. L., Meibom A., and McCoy T. J. 2001. Vesta, vestoids, and the howardite, eucrite, diogenite group: Relationships and the origin of spectral differences. *Meteoritics & Planetary Science* 36:761–781.

Christensen P. R., Bandfield J. L., Hamilton V. E., Howard D. A., Lane M. D., Piatek J. L., Ruff A. W., and Stefanov W. L. 2000. A thermal emission spectral library of rock-forming minerals. *Journal of Geophysical Research* 105:9735–9739.

Clark R. N. 1999. Chapter 1: Spectroscopy of rocks and minerals, and principles of spectroscopy. In *Manual of remote sensing, volume 3, remote sensing for the earth sciences*, edited by Rencz A. N. New York: John Wiley and Sons. pp. 3–58.

Clark R. N., Swayze G. A., Wise R., Livo E., Hoefen T., Kokaly R., Sutley S. J. 2007. USGS digital spectral library splib06a: US Geologic Survey, Digital Data Series 231. http://speclab.cr.usgs.gov/spectral-lib.html.

Cochran A. L. and Vilas F. 1998. The changing spectrum of Vesta: Rotationally resolved spectroscopy of pyroxene on the surface. *Icarus* 134:207–212.

Cochran A. L., Vilas F., Jarvis K. S., and Kelley M. S. 2004. Investigating the Vesta-vestoid-HED connection. *Icarus* 167: 360–368.

Consolmagno G. J. and Drake M. J. 1977. Composition and evolution of the eucrite parent body–Evidence from rare earth elements. *Geochimica et Cosmochimica Acta* 41:1271–1282.

Cooper B. L., Salisbury J. W., Killen R. M., and Potter A. E. 2002. Mid-infrared spectral features of rocks and their powders. *Journal of Geophysical Research* 107:5017, doi:10.1029/2000JE001462.

Cruikshank D. P., Tholen D. J., Hartmann W. K., Bell J. F., and Brown R. H. 1991. Three basaltic Earth-approaching asteroids and the source of the basaltic meteorites. *Icarus* 89:1–13.

Degewij J., Tedesco E. F., and Zellner B. 1979. Albedo and color contrasts on asteroid surfaces. *Icarus* 40:364–374.

Dotto E., Müller T. G., Barucci M. A., Encrenaz T., Knacke R. F., Lellouch E., Doressoundiram A., Crovisier J., Brucato J. R., Colangeli L., and Mennella V. 2000. ISO results on bright Main Belt asteroids: PHT-S observations. *Astronomy and Astrophysics* 358:1133–1141.

Drake M. J. 2001. The eucrite/Vesta story. *Meteoritics & Planetary Science* 36:501–513.

Feely K. C. and Christensen P. R. 1999. Quantitative compositional analysis using thermal emission spectroscopy: Application to igneous and metamorphic rocks. *Journal of Geophysical Research* 104:24,195–24,210.

Floran R. J., Prinz M., Hlava P. F., Keil K., Spettel B., and Wänke H. 1977. The Johnstown orthopyroxenite (diogenite) and its relationship to meteoritic cumulates. *Meteoritics* 12:226.

Floran R. J., Prinz M., Hlava P. F., Keil K., Spettel B., and Wänke H. 1981. Mineralogy, petrology, and trace element geochemistry of the Johnstown meteorite: A brecciated orthopyroxenite with siderophile and REE-rich components. *Geochimica et Cosmochimica Acta* 45:2385–2391.

Fuhrman M. and Papike J. J. 1981. Howardites and polymict eucrites: regolith samples from the eucrite parent body. Petrology of Bholghati, Bununu, Kapoeta, and ALHA76006. Proceedings, 12th Lunar and Planetary Science Conference. pp. 1257–1279.

Gaffey M. J. 1976. Spectral reflectance characteristics of the meteorite classes. *Journal of Geophysical Research* 81:905–920.

Gaffey M. J. 1997. Surface lithologic heterogeneity of asteroid 4 Vesta. *Icarus* 127:130–157.

Gaffey M. J. 2001. Asteroids: Does space weathering matter? (abstract #1587). 32nd Lunar and Planetary Science Conference. CD-ROM.

Golubeva L. F., Omarov S. Z., and Shestopalov D. I. 1983. Asteroid symmetry. I. surface mineralogies of Ceres and Vesta. *Soviet Astronomy* 27:83–87.

Grove C. I., Hook S. J., and Paylor II E. D. 1992. *Laboratory reflectance spectra of 160 minerals, 0.4 to 2.5 micrometers*. Pasadena, CA: NASA.

Hamilton V. E., Christensen P. R., and McSween Jr. H. Y. 1997. Determination of Martian meteorite lithologies and mineralogies using vibrational spectroscopy. *Journal of Geophysical Research* 102:25,593–25,603.

Hamilton V. E. and Christensen P. R. 2000. Determining the modal mineralogy of mafic and ultramafic igneous rocks using thermal emission spectroscopy. *Journal of Geophysical Research* 105: 9717–9733.

Helbert J., Moroz L., Maturilli A., Bischof A., Warell J., Sprague A., and Palomba E. 2007. A set of laboratory analogue materials for the MERTIS instrument on the ESA Bepi-Colombo mission to Mercury. *Advances in Space Research* 40:272–279.

Hiroi T., Pieters C. M., and Takeda H. 1994. Grain size of the surface regolith of asteroid 4 Vesta estimated from its reflectance spectrum in comparison with HED meteorites. *Meteoritics* 29: 394–396.

Hiroi T., Binzel R. P., Sunshine J. M., Pieters C. M., and Takeda H. 1995. Grain sizes and mineral compositions of surface regoliths of Vesta-like asteroids. *Icarus* 115:374–386.

Hiroi T., Pieters C. M., Vilas F., Sasaki S., Hamabe Y., and Kurahashi E. 2001. The mystery of the 506.5 nm feature of reflectance spectra of vesta and vestoids: evidence for space weathering? *Earth Planets Space* 53:1071–1075.

Hook S. J. 1998. ASTER spectral library. http://speclib.jpl.nasa.gov.

Hutchinson R. 2004. *Meteorites: A petrologic, chemical, and isotopic synthesis*. Cambridge: Cambridge University Press.

Johnson J. R., Hörz F., Lucey P. G., and Christensen P. R. 2002. Thermal infrared spectroscopy of experimentally shocked anorthosite and pyroxenite: Implications for remote sensing on Mars. *Journal of Geophysical Research* 107, doi:10.1029/2001JE001517.

Johnson J. R. and Hörz F. 2003. Visible/near-infrared spectra of experimentally shocked plagioclase feldspars. *Journal of Geophysical Research* 108, doi:10.1029/2003JE002127.

Keil K. 2002. Geological history of asteroid 4 Vesta: The "smallest terrestrial planet". In *Asteroids III*, edited by Bottke Jr., W. F., Cellino A., Paolicchi P., and Binzel R. P. Tucson: The University of Arizona Press. pp. 573–584.

Kitts K. and Lodders K. 1998. Survey and evaluation of eucrite bulk compositions. *Meteoritics & Planetary Science* 33:A197–A213.

Larson H. P. and Fink U. 1975. Infrared spectral observations of asteroid 4 Vesta. *Icarus* 26:420–427.

Li J.-Y., McFadden L. A., Thomas P. C., Mutchler M., Parker J. W., Young E. F., Russell C. T., Sykes M. V., and Schmidt B. E. 2008. Photometric mapping of asteroid (4) Vesta from HST observations (abstract #1391). 39th Lunar and Planetary Science Conference. CD-ROM.

Lim L. F., McConnochie T. H., Bell III J. F., and Hayward T. L. 2005. Thermal infrared (8–13 μm) spectra of 29 asteroids: The Cornell Mid-Infrared Asteroid Spectroscopy (MIDAS) Survey. *Icarus* 173:385–408.

Lyon R. J. P. 1965. Analysis of rocks by spectral infrared emission (8–25 microns). *Economic Geology* 60:717–736.

Maturilli A., Helbert J., and Moroz L. 2008. The Berlin emissivity database (BED). *Planetary and Space Science.* 56:420–425.

McCord T. B., Adams J. B., and Johnson T. V. 1970. Asteroid Vesta: spectral reflectivity and compositional implications. *Science* 168:1445–1447.

McFadden L. A., Thomas P. C., Carcich B., Mutchler M., Li, J., Bastien F., Hamilton D. P., Parker J., Young E. F., Sykes M. V., and Schmidt B. 2007. Observations of Vesta with HST-Wide Field Planetary Camera 2 in 2007. Proceedings, American Astronomical Society, 39th DPS meeting. Abstract #30.03.

McFadden L. A., Gaffey M. J., and Takeda H. 1981. The layered crust model and the surface of Vesta. Proceedings, 12th Lunar and Planetary Science Conference. pp. 685–687.

McFadden L. A., McCord T. B., and Pieters C. 1977. Vesta: The first pyroxene band from new spectroscopic measurements. *Icarus* 31:439–446.

Milam K. A., McSween Jr., H. Y., and Christensen, P. R. 2007. Plagioclase compositions derived from thermal emission spectra of compositionally complex mixtures: Implications for Martian feldspar mineralogy. *Journal of Geophysical Research* 112: E10005, doi:10.1029/2006JE002880.

Mittlefehldt D. W., McCoy T. J., Goodrich C. A., and Kracher A. 1998. Non-chondritic meteorites from asteroidal bodies. In *Planetary materials*, edited by Papike J. J. Washington D. C.: Mineralogical Society of America. pp. 4–1, 4–195.

Moroz L. V., Maturilli A., Helbert J., Sasaki S., Bischoff A., and Jessberger E. K. 2007. Mercury analogue materials: Spectral reflectance, its comparison with TIR spectral emission, and space weathering simulation experiment (abstract #1741). 38th Lunar and Planetary Science Conference. CD-ROM.

Mustard J. F. and Hays J. E. 1997. Effects of hyperfine particles on reflectance spectra from 0.3 to 25 mm. *Icarus* 125:145–163.

Pieters C. M. and McFadden L. A. 1994. Meteorite and asteroid reflectance spectroscopy: Clues to early solar system processes. *Annual Review of Earth and Planetary Sciences* 24:457–497.

Pieters C. M., Taylor L. A., Noble S. K., Keller L. P., Hapke B., Morris R. V., Allen C. C., McKay D. S., and Wentworth S. 2000. Space weathering on airless bodies: Resolving a mystery with lunar samples. *Meteoritics & Planetary Science* 35:1101–1107.

Pieters C. M. and Hiroi T. 2004. RELAB (Reflectance Experiment Laboratory): A NASA Multiuser Spectroscopy Facility (abstract #1720). 35th Lunar and Planetary Science Conference. CD-ROM.

Ramsey M. S. and Christensen P. R. 1998. Mineral abundance determination: Quantitative deconvolution of thermal infrared spectra. *Journal of Geophysical Research* 103:577–596.

Reid A. M., Buchanan P., Zolensky M. E., and Barrett R. A. 1990. The Bholghati howardite: Petrography and mineral chemistry. *Geochimica et Cosmochimica Acta* 54:2161–2166.

Rivkin A. S., McFadden L. A., Binzel R. P., and Sykes M. 2006. Rotationally-resolved spectroscopy of Vesta I: 2–4 μm region. *Icarus* 180:464-472.

Russell C. T., Coradini A., Christensen U., De Sanctis M. C., Feldman W. C., Jaumann R., Keller H. U., Konopliv A. S., McCord T. B., McFadden L. A., McSween H. Y., Mottola S., Neukum G., Pieters C. M., Prettyman T. H., Raymond C. A., Smith D. E., Sykes M. V., Williams B. G., Wise J., and Zuber M. T. 2004. Dawn: A journey in space and time. *Planetary and Space Science* 52:465–489.

Russell C. T., Capaccioni F., Coradini A., Christensen U., De Sanctis M. C., Feldman W. C., Jaumann R., Keller H. U., Konopliv A., McCord T. B., McFadden L. A., McSween H. Y., Mottola S., Neukum G., Pieters C. M., Prettyman T. H., Raymond C. A., Smith D. E., Sykes M. V., Williams B., and Zuber M. T. 2006. Dawn discovery mission to Vesta and Ceres: Present status. *Advances in Space Research.* 38:2043–2048.

Salisbury J. W., Walter L. S., and Vergo N. 1987. *Mid-infrared (2.1–25 μm) spectra of minerals*, 1st ed. Greenbelt, MD: USGS, Open-File Report 87–263.

Salisbury J. W., D' Aria D. M., and Jarosewich E. 1991. Mid-infrared (2.5–13.5 μm) reflectance spectra of powdered stony meteorites. *Icarus* 92:280–297.

Salisbury J. W. and Wald A. 1992. The role of volume scattering in reducing spectral contrast of Reststrahlen bands in spectra of powdered minerals. *Icarus* 96:121–128.

Salisbury J. W., Wald A., and D'Aria D. M. 1994. Thermal-infrared remote sensing and Kirchoff's Law 1. Laboratory measurements. *Journal of Geophysical Research* 99:11897–11911.

Schwartz J. M. and McCallum I. S. 2001. Evolution of the basaltic eucrite, Haraiya 6277 (abstract #2030). 32nd Lunar and Planetary Science Conference. CD-ROM.

Singer R. B. 1981. Near-infrared spectral reflectance of mineral mixtures: Systematic combinations of pyroxenes, olivine, and iron oxides. *Journal of Geophysical Research* 86:7967–7982.

Sprague A. L., Kozlowski R. W. H., Witteborn F. C., Cruikshank D. P., and Wooden D. H. 1994. Mercury: Evidence for anorthosite and basalt from mid-infrared (7.3–13.5 μm) spectroscopy. *Icarus* 109:156–167.

Thomas P. C., Binzel R. P., Gaffey M. J., Storrs A. D., Wells E. N., and Zellner B. H. 1997. Impact excavation on asteroid 4 Vesta: Hubble Space Telescope results. *Science* 277:1492–1495.

Vernazza P., Mothe-Diniz T., Barucci M. A., Birlan M., Carvano J. M., Strazzulla G., Fluchignoni M., and Migliorini A. 2005. Analysis of near-IR spectra of 1 Ceres and 4 Vesta, targets of the Dawn mission. *Astronomy & Astrophysics* 436:1113–1121.

Vilas F., Cochran A. L., and Jarvis K. S. 2000. Vesta and the Vestoids: A new rock group? *Icarus* 147:119–128.

Wisdom J. 1985. Meteorites may follow a chaotic route to Earth. *Nature* 315:731–733.

Wyatt M. B., Hamilton V. E., McSween Jr. H. Y., Christensen P. R., and Taylor L. A. 2001. Analysis of terrestrial and Martian volcanic compositions using thermal emission spectroscopy: 1. Determination of mineralogy, chemistry, and classification strategies. *Journal of Geophysical Research* 106:14,711–14,732.

Zellner B. H., Albrecht R., Binzel R. P., Gaffey M. J., Thomas P. C., Storrs A. D., and Wells E. N. 1997. Hubble Space Telescope images of asteroid 4 Vesta in 1994. *Icarus* 128:83–87.